Title

An experimental system and procedure of unsteady-state relative permeability test for gas hydrate-bearing sediments

Authors

Choi, Jeong-Hoon

Myshakin, Evgeniy M

Lei, Liang

et al.

Publication Date

2020-11-01

DOI

10.1016/j.jngse.2020.103545

Peer reviewed

Accepted for publication in *Journal of Natural Gas Science and Engineering*

An Experimental System and Procedure of Unsteady-State Relative Permeability Test for Gas Hydrate-Bearing Sediments

Jeong-Hoon Choi[1,2,**], Evgeniy M. Myshakin[1,2], Liang Lei[1,3], Timothy J. Kneafsey[4], and Yongkoo Seol[1,*]

[1] National Energy Technology Laboratory, U.S. Department of Energy, Morgantown, WV, USA

[2] Leidos Research Support Team, Morgantown, WV, USA

[3] Oak Ridge Institute for Science and Education, Morgantown, WV, USA

[4] Lawrence Berkeley National Laboratory, Berkeley, CA, USA

* Corresponding author: Yongkoo.Seol@netl.doe.gov, (304) 285-2029

**Corresponding author: Jeong.Choi@netl.doe.gov, (304) 285-2080

Abstract

Reliable estimations of the relative permeability of gas and water in hydrate-bearing sediments (HBS) and the dependency of the relative permeability on hydrate saturation are critical to predict the productivity of a hydrate reservoir. Yet, this remains poorly estimated owing to lack of experimental data associated with difficulties in conducting multiphase flow experiments in HBS. Recognizing the experimental challenges, this study intends to develop and validate a new experimental system and procedure of unsteady-state relative permeability test that can generate reliable and reproducible flow measurements in HBS. Gas hydrate is considered as a part of solid matrix in the sediment, so one of the challenges is to maintain a constant hydrate saturation, which is achieved in this experimental study using tight pressure-temperature (P-T) control near the hydrate stability boundary. The measured differential pressure across the specimen, methane injection flow rate, and volume of displaced brine are used to calculate the relative permeability by adopting a conventional Buckley-Leverett theory-based interpretation method. Residual brine saturation calculated for the hydrate-bearing specimen is higher than that of hydrate-free specimen, presumably due to decrease in pore size, increase in heterogeneity of solid matrix, and increase in size distribution of solid matrix and pore in the presence of hydrates. Further studies are necessary to represent the results of the unsteady-state flow experiment in HBS with a gas hydrate-dependent relative permeability model.

Keywords:

Unsteady-state relative permeability test, hydrate-bearing sediments, methane-brine relative permeability, residual saturation

1. Introduction

The volume of natural gas trapped in gas hydrates is reported to be enormous (Collett et al., 2009), which makes natural gas hydrates a potential energy resource in the future (Boswell, 2009; Makogon et al., 2007). Several onshore and offshore gas production tests have been conducted, e.g., Alaska North Slope, Mackenzie Delta, Nankai Trough, Gulf of Mexico, South China Sea, and so on, to examine the viability of gas production from hydrate reservoirs (Boswell et al., 2017; Dallimore et al., 2005; Li et al., 2018; Schoderbek et al., 2013; Yamamoto, 2013). To date the field tests are limited to short-term gas production from hydrate-bearing reservoirs. Numerical simulations that analyze multiphase flow through hydrate reservoirs remain a practical tool to evaluate the long-term production potential. Permeability of different fluid phases in hydrate reservoir is a fundamental input for such long-term numerical simulations (Anderson et al., 2011; Moridis et al., 2011; Myshakin et al., 2019; White et al., 2011).

Permeability of hydrate-bearing sediments (HBS) has two aspects. The first is the single-phase permeability, often called effective permeability with the presence of hydrates. Such permeability pertains to a measure of

absolute permeability change relative to the amount of hydrate contained in lab-made or natural HBS, and its experimental measurement has been reported by many studies (Delli and Grozic, 2014; Konno et al., 2015b; Kumar et al., 2010; Liang et al., 2011; Sakamoto et al., 2004; Seol et al., 2006; Yoneda et al., 2019). The second is the relative permeability of mobile phases (gas and water) that describes the competitive flow of both phases in HBS. Experimental measurements of such relative permeability have been reported by only a few studies (Ahn et al., 2005; Jaiswal, 2004; Johnson et al., 2011). However, some information was missing from these studies (e.g. detailed description of sample preparation, experimental systems, conditions, and/or procedures) that can be referred to for similar succeeding studies. The primary reason for the scarcity of gas-water relative permeability tests on HBS involves technical difficulties in limiting thermodynamic instability of gas hydrate in HBS during the multiphase flow (Johnson et al., 2011). The experimental difficulties have also led researchers to predict gas-water relative permeabilities in HBS using computational approaches (Mahabadi et al., 2016; Mahabadi and Jang, 2014; Singh et al., 2019; Singh et al., 2018), but the predicted results have not been vetted against robust laboratory measurements. Therefore, the development of an experimental setup, as well as an experimental procedure, is critical to obtain reliable and reproducible measurements that can be utilized to develop and validate relative permeability relationships in the presence of hydrates and to estimate relevant parameters for numerical

simulations of gas production from hydrate reservoirs.

This study first presents experimental challenges occurring during the relative permeability test on HBS. Experimental systems and procedures to mitigate the challenges and to conduct unsteady-state drainage relative permeability tests on HBS are then introduced. Thereafter, validation of the developed experimental methodology is performed, as well as the analysis of resulting relative permeabilities of methane and brine in the presence of gas hydrate. Some key research aspects, e.g., capillary heterogeneity that possibly results from pore size reduction/redistribution in presence of hydrate and thereby affects inferred relative permeability values, are discussed in respect of future studies at the end.

2. Experimental Challenges

Experimental challenges faced in conventional multiphase flow characterization of sediments become more complicated when gas hydrate exists in the pores of the medium. The primary reason for the complication is the dynamic change in thermodynamic equilibrium between gas hydrate and mobile phases that can cause either hydrate formation or dissociation upon applied pressure-temperature (P-T) condition which even changes to an extent across the length of a sample. This leads to a change in gas hydrate saturation in the pore space that alters the hydraulic characteristics of the original HBS. In the following sections, the experimental challenges that should be considered for reproducible relative permeability measurements of

HBS are addressed.

HBS Sample Preparation: Pressure cores retrieved from natural hydrate reservoirs are generally preferred for physical property characterization of HBS. However, there would be mechanical and P-T disturbances to the pressure cores that are hardly avoidable during coring, transferring, storing, and subsequent handling processes (Dai and Santamarina, 2014). In addition, the rare and expensive retrieved cores may not be representative for the whole reservoir considering large variability in lithofacies and compositions. Laboratory synthesized cores can be an alternative to the natural cores if they are adequately prepared under well-controlled P-T conditions, with representative sediment composition, hydrate saturation, and nature-like hydrate pore habit. The main challenge is to mimic the way hydrates form in natural sediments typically featuring pore-filling gas hydrate under excess-water conditions. A few sample preparation procedures have been proposed to synthesize the HBS having pore-filling, load-bearing, and/or patchy type hydrates under excess-water condition (Choi et al., 2014; Katsuki et al., 2007; Lei et al., 2019; Priest et al., 2009; Spangenberg et al., 2005; Yang et al., 2008).

Maintaining Hydrate Saturation/Measuring Gas and Liquid Saturations in HBS: Mobile phases (gas and water) flow through the sediment matrix (sediment particles and hydrates) either solely or jointly, and their

permeabilities need to be measured at each specific hydrate saturation so that full relative permeability contours of the three-phase system, i.e., hydrate + gas + liquid, can be built by consolidating all the relative permeability curves measured at different hydrate saturations (Seol and Kneafsey, 2011). Hydrate saturation and pore habit in the sediment, however, can vary depending on sediment characteristics (grain sizes, mineralogy, degrees of compaction, etc.) and thermodynamic reactions of hydrate, gas, and liquid under the applied experimental conditions, and these variations can influence the permeabilities (Dai and Seol, 2014; Kumar et al., 2010; Mahabadi et al., 2016; Mahabadi and Jang, 2014). Ideally, permeability measurement should be conducted under a condition where the three phases are thermodynamically stable, so that hydrate formation, dissociation, and redistribution can be avoided. Experimental systems should **1)** control P-T to keep hydrate disturbance as minimal as possible, **2)** monitor P-T changes in real time to allow timely P-T adjustments, and **3)** provide gas and liquid pre-saturated with each other to minimize molecular exchange between the two mobile phases and prevent hydrate from dissolving into liquid during permeability tests. In addition, to ensure the maintenance of overall hydrate saturation in the sediment during permeability tests, the systems should be able to detect the signs of extra hydrate formation and dissociation manifested through changes in effluent flow rates, so capabilities to measure such changes would be essential.

At a fixed hydrate saturation, the gas-liquid relative permeability is a

function of either gas or liquid saturation, and thus the mobile phase saturations in the presence of hydrate need to be measured during the test to derive the relative permeability relationship. To minimize possible errors in calculating mobile phase saturations, it is preferred to measure the volume of either mobile phase at the P-T condition applied to the test.

Maintaining Stable Back Pressure: Performing a relative permeability test requires an experimental system capable of maintaining stable back pressure. During the fluid flow, the pore pressure at the outlet face of a specimen is controlled by maintaining the pressure at the end point of downstream line (i.e., back pressure). In general, the pressure-valve-type back pressure regulator (BPR) is used for the back pressure control (Ahn et al., 2005; Jaiswal, 2004; Johnson et al., 2011), due to its advantages of no-limit on fluid-flow-through capacity and smaller size over syringe pressure pumps. However, in the gas-liquid relative permeability test on HBS, when the pressurized gas flows into the BPR and the gas pressure maintained by the BPR drops to atmospheric pressure at the pressure release point of BPR, the volume expansion of gas occurs that causes a temperature drop due to the Joule-Thompson effect. This can induce ice formation with concurrently exiting mobile liquid. The ice formation can partially or completely clog flow line ends and regulators, which leads to unstable back pressure control and excessive fluctuations in line pressure and differential pressure (ΔP). Therefore, a flow line should be designed to systematically limit excessive

gas volume expansion and preclude ice formation at the BPR for stable control of pore pressure and quality data collections.

Prevention of Clogging in Flow Lines from Unintended Hydrate Formation: Gas hydrate is known to form massive plugs in oil and gas pipelines, which causes blockages and pressure buildup. This is considered as a major operational hazard for the gas-oil industry (Deaton and Frost, 1946). The same type of flow line clogging remains challenging in bench-scale hydrate laboratory studies as well. The measurement of gas-liquid relative permeability in HBS inevitably introduces gas-liquid interfaces in flow lines, where hydrate can easily form to partially or completely clog the lines if the P-T condition falls within the hydrate stability zone. Partial or complete hydrate clogging of the lines can occur and interferes pressure transmission through experimental system, leading to false readings of transducers (line pressure, ΔP, and mass flow). The entire experimental system should, therefore, be divided by sections in accordance with the order of vulnerability to unintended hydrate formation, so that the individual sections can be inspected in the order at the occurrence of signs of clogging. This helps identify clogged spots with ease and remove them with minimal disturbance on the whole system-wise flow regime and hydrate stability in the specimen.

Prevention of Particle Loss from HBS Specimen: During the fluid flow, solids

in HBS specimen, including soil particles and hydrates, can migrate out of the specimen. Such migration alters the pore network of HBS specimen and can cause malfunctions in downstream regulators, transducers, and phase separators, as well as clogging in downstream flow lines, which adversely affects the quality of measured data for the permeability estimations. Several factors, such as flow velocity (or drag force), fluid chemistry, fines size (or weight), and pore throat size, should be carefully considered to inhibit or mitigate particle moving (Han et al., 2020; Oyeneyin et al., 1995; Sharma et al., 1992; Wan and Tokunaga, 2002). Preferably, to avoid the particle loss from the specimen and the damages to critical test equipment, direct preventive measures including filtration of migrating particles should be incorporated into the test setup, either on specimen or downstream flow lines depending on soil composition and fluid flow rates adopted during the permeability tests.

3. Relative Permeability Test Method

3.1. Overview

There are two methods generally adopted for the relative permeability measurement: steady-state and unsteady-state method. The steady-state method adopts simultaneous injections of two or more immiscible fluids through a specimen at a fixed injection ratio of the fluids until differential pressure and fluid saturations across the core are equilibrated. The equilibrated differential pressure and the volumetric injection rate of each

fluid are then used to calculate the relative permeability of the fluid at the fluid saturation measured. This “steady-state equilibrium flow test” should be repeated at different injection ratios of the fluids to form a relative permeability curve of each fluid over the range of fluid saturation. The steady-state method has advantages over the unsteady-state method, such that the relative permeability calculation is easily made with the effective permeability of each fluid calculated by a simple Darcy’s law at a given fluid saturation, and it is generally considered reliable as it involves simultaneous equilibrium of fluid flows rather than the displacement of one fluid by others, so that the test results are rarely affected by viscous instability (Maini et al., 1990; Peters, 2012). Disadvantages in the steady-state method include that the equilibria of pressure and fluid saturation (or fluid flows) at each injection ratio take a prolonged time, and thereby, the total duration of the flow test can be prohibitively extended with additional injection ratios. The difficulty in measuring phase saturations and consequent inaccuracy in measured saturations can also be another disadvantage of using the steady-state method (Honarpour et al., 1986).

In the unsteady-state method, a mobile phase present in a specimen is displaced by another immiscible mobile phase generally injected at a constant flow rate. The volume of the displaced phase and the differential pressure across the specimen are concurrently monitored during the injection of the displacing phase. The obtained data are then used to calculate the relative permeability curve of each mobile phase over a

saturation range of either displacing or displaced mobile phase. The "unsteady-state displacement test" can be completed quicker, which makes it more practical than the steady-state method, as it does not need a prolonged test time to attain equilibrated differential pressure and phase saturation. On the negative side, however, to obtain relative permeability curves, the unsteady-state method involves more intensive mathematical calculations relying on applying Buckley-Leverett (Buckley and Leverett, 1942) immiscible displacement theory-based methods, such as JBN (Johnson et al., 1959), JR (Jones and Roszelle, 1978), and Toth's (Toth et al., 2002) methods. These methods are developed based upon the assumptions that the specimen tested would be negligibly affected by 1) core heterogeneity, 2) capillary force, and 3) capillary end effects, and the relative permeabilities would then be calculated with monotonic fractional flow trends of displacing and displaced fluid phases. When non-monotonic fractional flows develop, which usually occur with severe heterogeneity in specimen, the calculated relative permeability curve can be discontinuous (or irregular) (Sigmund and McCaffery, 1979). Also, the methods, which neglect the capillary force in the relative permeability calculation, cannot inherently account for capillary heterogeneity and end effects that often appear in common cores during the displacement test. To minimize the effect of neglecting capillary force in the relative permeability calculation, the unsteady-state test should be conducted with a high injection (or displacing) flow rate that creates a differential pressure (across the specimen) large enough to overcome the

capillary force present in a specimen (Welge, 1952).

3.2. Selection of Relative Permeability Test Method

In general, neither of the two methods can provide both practicality and accuracy of relative permeability measurement at the same time. With the presence of hydrate in a specimen, the selection of an adequate relative permeability test method becomes more challenging. This selection should be made upon the comparative advantage of one method over the other with respects to several factors we considered in the previous section. However, for selection of the relative permeability test method in the presence of hydrate, the feasibility in measuring reliable mobile phase saturation is preferentially considered, since reliable mobile phase saturation measurement defines the quality of a relative permeability relationship. Measuring reliable phase saturation can be achieved in the unsteady-state method far more easily as explained below.

In the steady-state test method, a delicate estimation process (e.g., weighing or CT-scanning methods) is needed to measure the mobile phase saturations at the equilibrium condition. However, the presence of hydrate in the core specimen makes the measurement more complicated. For example, conventional weighing method generally requires removing cores from the pressure chamber for the estimation of difference in core weights whenever the equilibrium condition is reached at different injection ratios of mobile phases (Richardson et al., 1952), but the removal obviously causes

disturbance of hydrate present in the core. X-ray CT-scanning (Schembre and Kovscek, 2003; Vega and Kovscek, 2014) is often adopted to measure the saturations of mobile phases at the equilibrium condition, but the measurement would be challenging with the presence of hydrate due to the difficulty in obtaining the end member base scans under gas- and liquid-saturated conditions with identical locations of hydrate in pore space. Hydrate pore habit can evolve as liquid saturation changes (Choi et al., 2014; Lei et al., 2019), and as a result, the locations of hydrates can change. Another difficulty in adopting X-ray CT-scanning for mobile phase saturation measurements results from the similarity of gas hydrate and liquid (water) in both density and X-ray transparency. So, it would be very difficult to effectively separate hydrate and liquid (water) to estimate phase saturations (Lei et al., 2018).

In the unsteady-state test method, the measurement of mobile phase saturations can be attained with the production history of displaced mobile phase. Phase separators are conventionally used to monitor the amount of displaced phase over time. For HBS specimens, it can also be technically possible to reliably estimate mobile phase saturations in a specimen by monitoring the production history with a phase separator if overall hydrate saturation can be kept constant during the displacement test. In this study, therefore, the unsteady-state method is chosen over the steady-state method as a relative permeability measurement method for HBS specimen due to its relatively easy and quick estimation of phase saturations as well as

short overall test duration, even though it still shares the same challenges in coping with core heterogeneity, capillary force, and end effects that are present in hydrate-free sediments (HFS). Also, note that the short test duration of unsteady-state method can also be advantageous in reducing the possibility of hydrate saturation variation, which may increase under a prolonged coexistence of the three phases (hydrate, gas, and liquid) in a specimen.

4. Design of Experimental System

The experimental challenges and suggested mitigations to overcome these challenges are the main criteria to develop a practical experimental setup for the unsteady-state relative permeability test on HBS specimen. Figure 1 shows the experimental setup consisting of six major components: pressure chamber, differential pressure measurement system, pressure control system, temperature control system, flow control and measurement system, and immiscible fluid preparation system. The detailed descriptions and justifications for the choices of the experimental approach and systems developed are presented in the following subsections.

4.1. Pressure Chamber

A high-pressure aluminum chamber is incorporated into the system as a base testing cell for gas hydrate-bearing specimen preparation and conducting permeability tests. The pressure chamber (outer diameter of

12.1 cm × length of 43.8 cm) is equipped with a temperature controlling coolant jacket and capable of applying triaxial pressure conditions to the specimen: confining pressure through a stiff deformable rubber sleeve and axial pressure with a loading piston (Seol et al., 2014). The working pressure of the chamber is rated up to 21 MPa. The chamber uses a 5-mm thick rubber sleeve that is rigid enough to support a packed soil column and flexible enough to prevent injected fluid from flowing through the interface between its inner wall and the soil column (i.e., side-wall leakage) during the permeability test. Note that as shown in Figure 1, the pressure chamber is vertically set up during all the experimental procedures, especially to facilitate the liquid saturation of specimen and to minimize gas-liquid gravity segregation during the gas-liquid relative permeability test.

4.2. Differential Pressure Measurement System

A differential pressure transducer (DPT; 3051CD, Rosemount Inc.; accuracy of ±0.04% of span) is adopted to measure the differential pressure (ΔP) across the specimen during the permeability tests. The DPT is directly connected to the inlet and outlet faces of the specimen with tubing lines that are separate from the main flow lines (Figure 1). The separate ΔP tubing lines eliminate possible errors in the ΔP measurement, which occur when the ΔP tubing lines are connected to the main flow lines and the resistance of the portions of main flow lines that share the paths to/from the specimen with the ΔP tubing lines is large. In addition, a thin heating tip, made out of a

thermocouple with 0.25-mm diameter (TJC36-CASS-010U, Omega Inc.), is inserted into each end of ΔP tubing lines. The use of heating tips is to prevent the unintended hydrate formation in the ΔP tubing line ends by heating and thereby to ensure the measurement of ΔP, especially during the relative permeability test where the methane is injected into the brine-saturated specimen.

4.3. Pressure Control System

In order to independently control pore, radial, and axial pressures on the specimen, three syringe pumps (Pumps A, B, and C, respectively, in Figure 1; 500D, Teledyne ISCO) are connected to the corresponding pressure ports on the pressure chamber. Unlike radial and axial pressures, the pore pressure is designed to be controlled from both ends by injecting fluids on one end and simultaneously regulating the back pressure on the other end. A digitally-controlled dome-loaded back pressure regulator (BPR; DBPR-5HC, Coretest System Inc.) is installed at the end of downstream line to control the pore pressure. The BPR can control the pressure up to ~52 MPa with the allowable entry flow rate ranged from 0.01 to 15 ml/min. Note that absolute pressure transducers (Model 205, Setra Systems, Inc.; accuracy of ±0.073% of full scale) are used for the measurement of each pressure.

For the condition where both gas and liquid phases simultaneously flow out of the core specimen, a 1.5-liter liquid reservoir is installed before the BPR. The effluent flow is directed to the top port of the reservoir, and only

the liquid contained in the reservoir is released to the BPR through the bottom port of the reservoir. This reservoir helps improve the back-pressure control with reduced fluctuation by eliminating the chance of gas volume expansion and ice formation at the BPR. In this study, the reservoir is filled with a brine that has a salinity (8 wt % $CaCl_2$ solution) higher than that of the brine (5 wt % $CaCl_2$ solution) used to saturate the specimen and run single-phase (brine) permeability tests. With the brine having higher salinity, unintended hydrate formation can be avoided in the reservoir and BPR during the tests, since the test P-T condition is set near the hydrate stability boundary for 5 wt % $CaCl_2$ solution and the increase of salinity requires higher pressure/lower temperature for hydrate to form.

4.4. Temperature Control System

To prevent or minimize the change in gas hydrate saturation in the specimen during brine saturation process and permeability tests under a specific pressure, the temperatures of the specimen and surroundings need to be controlled. All the test equipment except for the gas cylinder is stationed inside an environmental chamber, within which the temperature is set at the actual specimen temperature (or test temperature). This helps avoid the hydrate formation and dissociation that can occur if the temperature of injected fluid is different from that of specimen.

The temperatue of the specimen can be regulated further by a cooling bath that circulates coolant through an external jacket covering the main

body of the pressure chamber. The cooling bath is especially useful for adjusting specimen temperature below that of environmental chamber during hydrate formation and precisely controlling specimen temperature during the saturation process and permeability tests. As a note, to reduce the impact of ambient temperature fluctuation of the environmental chamber on specimen temperature, multiple layers of insulation material are placed around the cooling jacket of the pressure chamber. The specimen temperature is monitored by a K-type thermocouple (Omega Inc.) embedded 2.54-cm deep into the bottom of specimen. The standard deviation of specimen temperature readings calibrated in the range of 0 to 50 °C is about 0.05 °C.

The flow lines are covered with insulation material to help inhibit the lines from clogging by unintended hydrate formation that can occur if the lines are directly exposed to cooling air circulation. Inside the environmental chamber, it is always possible to have cooling air flow that comes directly from the air conditioning unit. If any signs of clogging appear by unintended hydrate formation, such as increasing line pressure, the suspected section of flow lines can be warmed with external heat sources to dissociate the hydrate. Note that the hydrate clogging causing line pressure increase usually happens on the downstream side where gas and liquid concurrently flow especially during the relative permeability test.

4.5. Flow Control and Measurement System

The pore fluid injection pump (Pump A in Figure 1 with 500-ml volume) is used to supply gas (methane) into the specimen during the hydrate formation and to inject liquid (brine) during the saturation of the hydrate-formed specimen and the single-phase (brine) permeability test. The pore fluid injection pump maintains **1)** pore pressure constant during the hydrate formation with the outlet port of the pressure chamber closed or **2)** injection flow rates constant during the single-phase permeability test together with the back-pressure regulator (BPR) at the end of downstream line. The volume capacity of the pump should be sufficient to complete hydrate formation, brine injection, or a single-phase (brine) permeability test without interruptions for refilling with the corresponding fluid. Note that during the hydrate formation, brine saturation, and single-phase (brine) permeability tests, the methane and brine flowing out of the pump are directed to enter the vertically-standing specimen from the bottom.

During a gas-liquid drainage relative permeability test, injecting displacing fluid (methane) needs to continue without interruptions until the ΔP across the specimen and accumulated volume of displaced fluid (brine) become stabilized. For the continuing injection of methane gas at a constant flow rate, a high-pressure mini Coriolis mass flow controller (MFC; M12V10I, Bronkhorst USA Inc.; accuracy of ±0.5% of reading for gas), directly connected to a gas supply cylinder, is used to regulate the methane injection into the brine-saturated specimen. The MFC directly regulates mass flow rates and converts the regulated mass flow rates into volumetric flow rates

based on flowing fluid (methane) density that the MFC measures. It should be noted that the accuracy of Coriolis MFC is generally known to be higher than commonly used thermal MFC, so the reliability of measured ΔP and accumulated volume of displaced fluid for the targeted flow rate can be improved with the Coriolis type. The regulated methane flow then enters the specimen from the top.

The volume measurement of displaced fluid flowing out of the specimen needs to be made during the gas-liquid relative permeability test. The measured fluid volumes are base inputs to estimate fluid saturations in the specimen. A general phase separator can be used for the volume measurement with visual volume reading or post-weighing the collected fluid, but such subjective or indirect measurements can include errors. In this study, a high-pressure sonic phase separator (SPS; two-phase; SFS-032, Coretest System Inc.) is used between the pressure chamber and the liquid (brine) reservoir on the downstream side for high accuracy volume measurement (resolution of 0.06 ml) of displaced fluid (brine) under a predetermined P-T condition. Sonic reflection from the interface between two immiscible effluent fluids (methane + brine) allows continuous volume measurements of displaced fluid. The accurate measurement of volume of displaced fluid reduces the error in estimating mobile phase saturations that govern the relative permeabilities of the mobile phases.

The volume of effluent fluids (methane + brine) flowing from the specimen can be estimated using a high-pressure Coriolis mass flow meter

(MFM; M12, Bronkhorst USA Inc.; accuracy of ±0.2% and ±0.5% of reading for liquid and gas, respectively), which is connected either to the upper outlet port of the SPS for drainage relative permeability test or to the lower outlet port for imbibition test. For this study, we use the drainage test configuration. With the drainage test configuration, only methane gas that occupies the upper part of the SPS can exit the SPS through the upper outlet port as soon as the effluent fluids flowing from the specimen enters the SPS through the upper inlet port. The volume of methane exiting the SPS should be equivalent to that of effluent fluids entering the SPS, because the pressure of the SPS is maintained constant by a constant back pressure. Therefore, the mass flow rate and density of the exiting methane, measured by the MFM, can be used to calculate the volume of effluent fluids ("methane + brine") over time. With the volume of effluent fluids ("methane + brine") estimated by the MFM and the volume of displaced fluid ("brine" in drainage test) measured by the SPS, the volume of displacing fluid ("methane" in drainage test) entering the SPS can be calculated as well. Also, unintended hydrate formation and dissociation in the specimen and flow lines that possibly occur during the tests can be noticed by monitoring the change in the mass flow rate with the MFM.

4.6. Immiscible Fluid Preparation System

It is important to keep the hydrate saturation of a HBS specimen steady during the entire course of experiment, including the step of

saturating specimen with liquid (brine), single-phase (brine) permeability test, and gas-liquid (methane-brine) relative permeability test. To avoid hydrate saturation changes, the methane and brine need to be pre-saturated with each other under the test P-T condition before their injection into the specimen, which also allows for immiscible displacement condition during the relative permeability test. Another pump (Pump D; 500D, Teledyne ISCO), named the fluid mixing pump, is implemented into the test setup to saturate the brine with methane before the brine is injected into the specimen for the brine saturation of specimen and the single-phase permeability test. The fluid mixing pump (Pump D) is first filled with the brine and connected to the pore fluid injection pump (Pump A) that contains methane. Then, the connected two pumps exchange the two fluids back and forth to equilibrate the two fluids with each other. After three times of fluid exchanges, the residual methane is removed to the fluid mixing pump, and only the methane-saturated brine is left in the pore fluid injection pump for its injection into the specimen. To moisten methane with water vapor for the gas-liquid relative permeability test, a 50-ml reservoir half-filled with brine is installed on the outlet side of the MFC. The methane flow regulated by the MFC is directed to flow into the bottom of the reservoir, pass through the brine, and then exit through the top, so that the methane becomes damp before entering the specimen.

5. Test Procedure

A test procedure has been developed to sequentially conduct single-phase (brine) permeability and gas-liquid (methane-brine) drainage relative permeability tests on a single specimen with and without gas hydrate using the developed experimental system. The following sections introduce the details of the test procedure that include a specimen preparation method as well as the sequence of permeability tests.

5.1. Hydrate-Bearing Specimen Preparation

A HBS specimen is prepared to have a hydrate pore habit that is typically found in natural HBS, i.e., pore-filling, load-bearing or patchy type, rather than cementing type (Konno et al., 2015a; Santamarina et al., 2015). In the following subsections, the procedure of specimen preparation is described step by step from the host sediment formation to the brine saturation of the HBS specimen.

5.1.1. Host Sediment Preparation

As a main substrate for the HBS specimen, dry silica sand (F110; median particle size, D_{50} = 120 μm) is mixed with kaolinite clay (5% by weight; D_{50} = 1 μm). Kaolinite clay is added to mimic natural sandy sediments, which generally contain fine particles (Boswell et al., 2009; Ito et al., 2015). Deionized water is added to form a partially-saturated sediment mixture with a water content of 9.3 wt %. The amount of water added in the

547 mixture determines the initial hydrate saturation of the specimen, i.e., 40-
548 45% in the sediment mixture with 0.34-0.37 porosity. A paper filter (Grade
549 P5; particle retention = 5 to 10 μm; Herzberg flow rate = 60 ml/min, which is
550 equivalent to the permeability of 39.4 mD) is placed on top of the bottom
551 end cap of the testing cell to prevent the loss of soil particles and hydrates
552 during the subsequent soil packing, specimen saturation, and permeability
553 tests. As a note, more caution should, however, be taken to apply such
554 filters directly on the specimen especially when a highly permeable
555 specimen is tested and the fine content in the specimen is high, because the
556 permeability of the filter can cause a significant underestimation in the
557 permeability measurement of specimen and the filters can be clogged by
558 fines during fluid flow. The partially-saturated sediment mixture is then
559 packed into a round rubber sleeve (I.D. = 50.8 mm) sitting on the bottom
560 end cap of the testing cell. The dimensions and index properties of the
561 specimen obtained after packing are shown in Table 1.
562

563 **5.1.2. Hydrate Formation**

564 Methane hydrate is formed in the specimen by employing the brine-
565 injection and warming-cooling method (Choi et al., 2014). The hydrate
566 formation method consists of three main steps: **1)** initial hydrate formation
567 in the partially water (not brine) saturated specimen by raising the pore
568 pressure (u) to 6.89 MPa with methane injection (i.e., under excess-gas
569 condition), lowering the specimen temperature to ~4 °C, at which the P-T of

570 specimen is positioned well within the hydrate stability boundary for water,
571 and subsequently providing the specimen with methane keeping the pore
572 pressure constant; **2)** slow injection of methane-charged brine (5 wt % $CaCl_2$
573 solution; ~5 pore volumes) into the HBS specimen under a controlled P-T
574 condition of 6.89 MPa and ~8 °C, which is still within the hydrate stability
575 boundary for water; and **3)** a temperature warming-cooling cycle (~12 °C to
576 ~2 °C) on the brine-filled HBS specimen in a closed system. With this
577 method, hydrate forms in the specimen filling in brine-saturated pore spaces,
578 mostly being off sediment particle contacts, which was proven with wave
579 velocity measurements in our previous study (Choi et al., 2014). Once the
580 warming-cooling step is completed as shown in Figure 2, the pore pressure is
581 adjusted to 6.89 MPa with methane-saturated brine injection or pore brine
582 release (depending on the pore pressure attained after the warming-cooling
583 step), while the temperature to ~8 °C. The P-T condition of 6.89 MPa and ~8
584 °C is selected to position the system condition slightly outside the hydrate
585 stability boundary for 5 wt % $CaCl_2$ solution (6.89 MPa and 7.7 °C). The
586 selection of the P-T condition is intended to prevent or minimize the change
587 in overall hydrate saturation of the specimen during the brine injection and
588 the subsequent permeability tests (Choi et al., 2014). During hydrate
589 formation, the temperature of environmental chamber is set at ~8 °C, and
590 the effective confining stress (σ'_o) is maintained at ≤ 0.69 MPa. After the
591 completion of hydrate formation and P-T adjustment, additional methane-
592 charged brine (~5 pore volumes) is injected into the HBS specimen to ensure

its full saturation with the brine. Table 1 shows the P-T condition and hydrate saturation (S_h) of the specimen before the permeability tests. Note that the hydrate saturation in the specimen is estimated with the amount of gas collected during the later hydrate dissociation conducted after the completion of permeability tests.

5.2. Permeability Tests

The sequence of steps applied in the permeability tests includes: **1)** an effective permeability test with brine on the HBS specimen; **2)** an unsteady-state drainage relative permeability test on the HBS specimen; **3)** dissociation of hydrate and re-saturation of the HFS specimen with brine (~5 pore volumes); **4)** an intrinsic permeability test with brine on the HFS specimen; and **5)** an unsteady-state drainage relative permeability test on the HFS specimen. For all the permeability tests, the P-T condition of specimen is set at 6.89 MPa and ~8 °C.

5.2.1. Single-Phase Permeability Test

Steady-state single-phase permeability tests (i.e., effective and intrinsic permeability tests on HBS and HFS specimens, respectively) are conducted by injecting methane-charged brine into the brine-saturated specimen. The brine is injected into the specimen at multiple volumetric flow rates (q; 0.5 to 8 ml/min) by the pore fluid injection pump (Pump A). The ΔP across the specimen is measured at each flow rate, when a stable ΔP

level is attained (Figure 3).

5.2.2. Gas-Liquid Relative Permeability Test

Gas-liquid relative permeability tests on the HBS and HFS specimens are conducted based on the unsteady-state drainage method. Moistened methane is injected into the brine-saturated specimen at a flow rate of 8 ml/min regulated by the MFC. The methane injection flow rate mimics the gas flow rate (normalized to flow through an interface area unit [m^2]) predicted to occur near the wellbore of a producing gas hydrate reservoir, such as the Site NGHP-02-16 in Area-B of the Krishna-Godavari Basin in offshore India (Myshakin et al., 2019). Key experimental data to collect during the relative permeability tests include the ΔP and the volume of brine displaced by the injected methane, which are monitored until their variations become stabilized.

6. Results

Fundamental experimental data, such as pressure, temperature, and mass flow rate, monitored during single-phase permeability and gas-liquid relative permeability tests are provided to present the reliability of the proposed experimental system and procedures. On the other hand, key experimental data, such as ΔP and volume of displaced brine, are interpreted to obtain the permeabilities, and the results are compared to reveal the effects of hydrate on the permeabilities and analyzed to understand their

639 physical implications to the fluid flow in the HBS.

640

641 **6.1. Single-Phase (Brine) Permeability Test**

642 The single-phase permeability of the specimen, either effective or
643 intrinsic permeability depending on the presence of hydrate, is further used
644 as a base to estimate relative permeability of mobile fluids. Figure 3 shows
645 the ΔP across the specimens measured at various injection flow rates (q)
646 during the single-phase (brine) permeability tests. It is shown in Figure 3
647 that ΔP increases linearly with increasing q for both HBS and HFS specimens.
648 The linearity with R^2-values of > 0.990 reflects the pore structure stably
649 conserved during the brine injection, meaning that under the adopted P-T
650 condition, noticeable changes in hydrate saturation and hydrate pore habit
651 are prevented or minimized in the specimen. Also, the linearity suggests
652 that the clogging of the specimen and paper filter by fines (clay particles)
653 migration or hydrate formation is likely avoided during the tests. Note that
654 the flocculation of clay particles in the $CaCl_2$ brine possibly helps limit the
655 clay migration under the applied injection flow rates.

656 The ΔP and q data for each specimen are then used to calculate their
657 single-phase permeabilities (k) using Darcy's law as follows:

658 $$k = \frac{q\mu L}{A\Delta P} \quad (1)$$

659 where μ = dynamic viscosity of fluid; L = length of specimen; and A = cross-
660 section area of specimen. Effective and intrinsic permeabilities are
661 calculated at different flow rates and averaged as shown in Table 2. As

662 expected, the presence of hydrates (S_h = 42.0%) in the specimen reduces
663 the permeability of specimen. The permeability reduction index (N) of 3.09,
664 calculated from $k_e/k_0 = (1 - S_h)^N$ (where k_e and k_0 = effective and intrinsic
665 permeabilities, respectively), indicates that patchy type hydrates with a
666 weak cementation with surrounding soil particles may exist in the specimen
667 (Dai and Seol, 2014). As a note, applying paper filters (with the permeability
668 of 39.4 mD) on both ends of specimen leads to negligible errors in the
669 estimation of permeability in this study. Accounting for the paper filters
670 results in actual permeabilities of the HBS and HFS specimen being about
671 0.9% and 5.0% higher than those shown in Table 2, respectively.
672
673 **6.2. Gas-Liquid Relative Permeability Test**
674 **6.2.1. P-T Monitoring**
675 During the relative permeability test, unintended hydrate formation or
676 dissociation can occur in the specimen when the P-T condition of the
677 specimen drifts into or out of the hydrate stability zone. Figure 4 shows the
678 outlet pore pressure and temperature of HBS specimen monitored during the
679 relative permeability test. As shown, the monitored P-T values fluctuate, and
680 their average values (6.94 MPa and 8.2 °C) deviate from the targeted P-T
681 (6.89 MPa and ~8 °C). However, the overall trend of monitored P-T moves
682 within the standard deviation of 7 kPa and 0.1 °C, and their deviation from
683 the targeted P-T is less than +0.05 MPa and +0.2 °C, which reveal that the
684 outlet pore pressure and temperature of specimen are stably controlled.

Note that there are two noticeable features observed in pore pressure and temperature data. Several small spikes on outlet pore pressure indicate short-lived flow pathway blockages, which seem to be caused by unintended hydrate formations in the downstream flow line when the temperature cycle of environmental chamber reaches its cooling trough. Moderate cyclic changes in specimen temperature are caused by fluctuations of ambient temperature in the environmental chamber.

6.2.2. Mass Flow Rate Monitoring

Figure 5 shows the mass flow rate of methane (in green) vented from the sonic phase separator (SPS) during the relative permeability test with the HBS specimen. While there are several small spikes in the mass flow rate resulting from temporary clogging episodes with unintended limited hydrate formation, its overall trend (average mass flow rate = 0.55 g/min; standard deviation = 0.03 g/min) is consistent with the methane injection rate (in red) into the specimen throughout the test. The consistency indicates that hydrate saturation is well maintained.

6.2.3. Differential Pressure and Volume of Displaced Brine

Figure 6 shows the variation in ΔP and the accumulated volume of brine displaced from the brine-saturated specimen (V_k) by methane injection. The early increase in ΔP occurs because of the entry of the residual brine from injection tubing line into the brine-saturated specimen. Note that the

injection tubing line is fully filled with brine after the previous single-phase (brine) permeability test. Once the methane reaches the inlet face of the specimen and the capillary entry pressure is overcome, methane starts to flow into the specimen. As soon as methane starts flowing in and displacing the brine from the specimen, ΔP drops rapidly. The curves of the drop of ΔP and the increase in accumulated volume of displaced brine (V_k) gradually flatten as the methane injection progresses. The data curves of HBS and HFS specimens become nearly flat after about 8 and 4.5 pore volumes of methane injection, respectively.

The HFS specimen, mostly composed of F110 sand with the median particle size (D_{50}) of 120 μm, has the averaged pore throat size of about 12 μm, i.e., about one tenth of diameter of sediment particle (Hunt et al., 1988), and its capillary entry pressure can be estimated about 23 kPa ($P_{c,e} \approx 2\sigma/r_t$, where σ = interfacial tension between methane and brine, ~70 mN/m and r_t = radius of pore throat, ~6 μm), which is equivalent to the ΔP at the onset of methane entry into the specimen as shown in Figure 6b. This indicates the paper filter used on the specimen may not have much influence on the early ΔP development for the HFS specimen, which is also backed up by the particle retention size (or pore size) of the paper filter (5 to 10 μm) that is close to the pore throat size of the specimen (~12 μm). Also note that the paper filter may have no influence on the early ΔP development for the HBS specimen (Figure 6a), since the averaged pore throat size of the specimen with the presence of hydrate is smaller than the particle retention size of the

731 paper filter.

732 To accurately estimate the saturation of each fluid phase in the
733 specimen, the arrival time of injected methane at the inlet face of specimen
734 must be known. The arrival time of the methane can be estimated by
735 counting the time that the V_k (measured by the SPS from the start of
736 methane injection) takes to become equivalent to the known internal volume
737 of the injection tubing line up to the inlet face of the specimen (note: the
738 injection tubing line is fully filled with brine at the start of methane injection).
739 The estimated arrival times of injected methane are ~26 and ~19 seconds
740 for the tests on the HBS and HFS specimens, respectively, as shown in Figure
741 6. The discrepancy in the arrival time (between ~26 and ~19 seconds) can
742 occur when the time interval to reach the targeted injection flow rate (8 ml/
743 min) is different. The time interval varies depending on the flow-controlling
744 parameters set in the MFC.

745 The time for the injected methane to break through the specimen can
746 easily be recognized with the V_k plot where the early linear increase of V_k
747 turns into the nonlinear increase (as indicated in Figure 6, at 78 and 132
748 seconds on the V_k data of HBS and HFS specimens, respectively).
749 Recognizing the break-through point is important, since the calculations of
750 unsteady-state relative permeability based on Buckley-Leverett theory are
751 made with the analysis of fractional flow data that are only obtained after
752 the break-through.

753 Note that while the ΔP data are measured with the DPT located right on

754 the specimen, the V_k data are measured with the SPS located on the
755 downstream side away from the specimen. The V_k reflects the saturations of
756 mobile fluids in the specimen that influence the ΔP. However, the V_k is
757 measured with a time delay relative to the corresponding ΔP, due to the
758 difference in data measurement location. The two data sets of ΔP and V_k,
759 therefore, need a temporal matching to each other (synchronization). The
760 time delay can be estimated by measuring the travel time of effluent fluid
761 from the outlet face of specimen to the SPS. The measurement of the travel
762 time can be experimentally attainable by counting the time elapsed for "the
763 accumulated volume of effluent fluid (brine) that has flowed out of the
764 specimen since the arrival of the methane at the inlet face of the specimen"
765 to become equivalent to "the known internal volume of tubing line from the
766 outlet face of the specimen to the inlet port of the SPS". In the current test
767 setup, the accumulated volume of effluent fluid can be measured by the
768 MFM. The measured travel time (i.e., time delay) is about 42 and 43 seconds
769 for the tests on HBS and HFS specimens, respectively. Consequently, in case
770 of the test on the HBS specimen (Figure 6a), the V_k at 68 seconds (= 26
771 seconds + 42 seconds) becomes the initial data point for the temporal
772 matching with the ΔP at 26 seconds that corresponds to the arrival of
773 methane front at the inlet face of the specimen. The ΔP and V_k data
774 collected at and after the temporal matching points are used for the
775 subsequent relative permeability calculation.
776

6.2.4. Relative Permeability Curves

Toth's method, a direct interpretation method (Toth et al., 1998; Toth et al., 2002) developed based on Buckley-Leverett theory, is adopted for the relative permeability calculation. Toth's method employs four statistical parameters (a, b, a_1, and b_1) obtained from two linear regression equations, which are created using the data of accumulated volume of displaced fluid (V_k; brine) and differential pressure (ΔP) across the specimen obtained at and after the break-through of the fluid (methane) injected into the specimen:

$$\frac{V_i(t)}{V_k(t)} = a + b\left(\frac{V_i(t)}{V_p}\right) (t \geq t_a) \quad (2)$$

$$\Delta P(t) = a_1 \left(\frac{V_i(t)}{V_k(t)}\right)^{b_1} (t \geq t_a)(linearly\ fitted \in \log - \log scale) \quad (3)$$

where V_i = accumulated volume of injected fluid (methane); V_p = pore volume; t = time elapsed from the onset of the invasion of injected fluid (methane) into the specimen; and t_a = break-through time. With the linear data regression, Toth's method is considered more simple and applicable, compared to the conventional methods that involve non-linear regressions and graphical techniques (Johnson et al., 1959; Jones and Roszelle, 1978), particularly when data fluctuation is evident as shown in Figure 6. The data regressions to obtain the Toth's statistical parameters are shown in Figure 7, and the obtained parameters are listed in Table 2 along with other parameters necessary to calculate relative permeability curves, such as

specimen dimension, effective porosity, flow rate of fluid (methane) injection, initial saturation of displacing fluid (methane), dynamic viscosities of fluids (methane and brine), and absolute permeabilities (effective and intrinsic permeability for HBS and HFS specimens, respectively). Relative permeability curves are then calculated, as shown in Figure 8, by plugging the parameters into relevant Toth's equations (Toth et al., 2002).

$$S_{d,2}=b\left[\frac{\frac{V_i(t)}{V_p}}{a+b\frac{V_i(t)}{V_p}}\right]^2+S_{d,i} \quad (4)$$

$$M_{d,2}=\frac{\left[a+b\frac{V_i(t)}{V_p}\right]^2}{a}-1 \quad (5)$$

$$f_{d,2}=\frac{M_{d,2}}{M_{d,2}+1} \quad (6)$$

$$f_{k,2}=\frac{1}{M_{d,2}+1} \quad (7)$$

$$Y\left(S_{d,2}\right)=\frac{qL}{kA\,a_1+\left(1-b_1\right)\left(\frac{V_i(t)}{V_p}\right)^{b_1}} \quad (8)$$

$$k_{r,d}=\mu_d f_{d,2} Y\left(S_{d,2}\right) \quad (9)$$

$$k_{r,k}=\mu_k f_{k,2} Y\left(S_{d,2}\right) \quad (10)$$

where $S_{d,2}$ = saturation of displacing fluid (methane) at outlet face of specimen; $S_{d,i}$ = initial saturation of displacing fluid (methane); $M_{d,2}$ = mobility ratio of displacing fluid (methane) at outlet face of specimen; $f_{d,2}$ and

$f_{k,2}$ = fractional fluid flows of displacing (methane) and displaced (brine) fluids, respectively; k = absolute permeability (i.e., effective and intrinsic permeabilities for HBS and HFS specimens, respectively); $Y(S_{d,2})$ = total mobility function; $k_{r,d}$ and $k_{r,k}$ = relative permeabilities of displacing (methane) and displaced (brine) fluids, respectively; and μ_d and μ_k = dynamic viscosities of displacing (methane) and displaced (brine) fluids, respectively.

As shown in Figure 8 (solid lines), the residual brine saturations obtained with about 8 and 4.5 pore volumes (V_i/V_p) of methane injection are 0.933 and 0.696 for the HBS (S_h = 42.0%) and HFS specimen, respectively. The residual brine saturation of HBS specimen is higher than that of HFS specimen, even though more of methane (8 pore volumes) is injected into the HBS specimen. The steeper drop and rise of brine and methane relative permeability, respectively, are also observed for the HBS specimen with the earlier attainment of the residual state of brine in the specimen.

Meanwhile, using the same Toth's fitting parameters, relative permeability values are extrapolated (dotted lines in Figure 8) as if 100 pore volumes of methane is injected. As a result, the residual brine saturations are reduced to 0.932 and 0.656 for HBS (S_h = 42.0%) and HFS specimen, respectively. The reduction in the residual brine saturation after the virtually extended methane injection appears to be negligible, suggesting that the actual volumes of methane injection (~8 and ~4.5 pore volumes for HBS and HFS specimen, respectively) would be reasonable to bring the brine residing in the specimen to its residual state.

7. Discussion

Maintaining the hydrate saturation of the HBS specimen during the relative permeability test is the most challenging task in this study. We discuss how it is accomplished with the controlled P-T condition. In addition, we discuss the possible cause and remedy of the high residual brine saturation observed in the relative permeability curve of the HBS specimen.

7.1. Preservation of Hydrate Saturation with Controlled P-T Condition

In Figure 2, the P-T condition at the outlet face of the HBS specimen during the relative permeability test is plotted in comparison with that observed during the warming-cooling step of hydrate formation in the specimen within the closed system. As shown in the inset in Figure 2, during the warming step, a noticeable pressure increase, i.e., an indication of hydrate dissociation, appears to be delayed maintaining ~6.89 MPa until the temperature reaches ~8.4 °C, although the P-T is already outside the hydrate stability boundary (~7.7 °C at 6.89 MPa). This delay may occur because of the combined effects of: **1)** brine salinity reduction associated with fresh water release by minor or localized hydrate dissociations, **2)** minor pressure increase related to gas release, and **3)** temperature decrease owing to the endothermic nature of the hydrate dissociation reaction (Choi et al., 2014). Minor or localized hydrate dissociation-reformation processes occur

quickly leading to the delay in dissociation, since there is no induction time associated with hydrate lattice formation when water bearing the “memory effect” is promptly available from a previous occurrence of dissociation (Myshakin et al., 2009). Once the driving force of hydrate decomposition created by the temperature increase becomes large enough to break such thermodynamic metastable condition, the continuous hydrate dissociation occurs.

The P-T conditions of the HBS specimen throughout the relative permeability test (Figure 2 inset; purple and red plots for inlet and outlet sides of the specimen, respectively) are outside the hydrate stability zone, but they do not reach the thresholding P-T condition (~8.4 °C at 6.89 MPa) that initiates the continuous hydrate dissociation during the warming step. The metastable condition also likely occurs and limits hydrate dissociation, preventing noticeable changes in hydrate saturation at both inlet and outlet face of the specimen during the relative permeability test. All of this indicates that under the P-T condition of 6.89-7.10 MPa and 7.8-8.4 °C, the gas-liquid multiphase flow test is executed without significant unintended hydrate formation and dissociation in the HBS specimen, especially when the 5 wt % $CaCl_2$ brine is used as a liquid phase to saturate the specimen. The liquid phase salinity buffers hydrate stability by creating a thermodynamic metastable condition, allowing the relative permeability measurements.

As an additional piece of evidence of the preservation of hydrate saturation with controlled P-T condition, it should also be noted that the

883 methane amount consumed during the initial hydrate formation (~0.338
884 mol) appears to closely match that collected during the hydrate dissociation
885 conducted after the relative permeability test (~0.326 mol). The hydrate
886 saturations calculated based on the measured methane amounts are about
887 43.6% and 42.0% for the cases after initial hydrate formation and after
888 relative permeability test, respectively. When all possible sources of
889 experimental error are taken into consideration, the difference seems to be
890 negligible. Therefore, it can possibly claimed that the hydrate saturation of
891 the specimen has been preserved throughout the brine saturation, single-
892 phase (brine) permeability test, and relative permeability test under the
893 controlled P-T condition.
894
895 **7.2. Residual Brine Saturation of HBS Specimen**
896 The relative permeability curves (Figure 8) show that the residual brine
897 saturation of the HBS specimen is higher than that of the HFS specimen. The
898 presence of hydrate in the specimen reduces pore size while increasing total
899 surface area of solid matrix (sediment and hydrate). Both of these factors
900 increase the capillary retention of brine. As seen in imaging studies (Rees et
901 al., 2011; Seol and Kneafsey, 2011), the hydrate increases sediment
902 heterogeneity, solid matrix size distribution, and pore size distribution, which
903 can also lower displacement efficiency. Meanwhile, the low viscosity ratio of
904 injected methane to brine ($M = 8.452 \times 10^{-3} < 1$) inherently results in
905 viscous instability that would incur preferential pathways (i.e., fingering) in

906 the saturated sediment. The advance of displacing fluid (methane) in a
907 fingering pattern leads to an early break-through and in turn, lowers break-
908 through production of displaced fluid (brine), contributing to the low
909 displacement efficiency. Once gas pathways are developed, it is difficult to
910 improve such low displacement efficiency any further.

911 Relative permeability is also dependent on injection flow rates when
912 the viscous instability and capillary heterogeneity of a porous medium are
913 significant (Huppler, 1970; Peters and Khataniar, 1987). A capillary number
914 of ~3.316 × 10^{-8} ($Nc = \mu v / \sigma$, where μ = dynamic viscosity of displacing
915 phase, i.e., methane, 1.234 × 10^{-5} Pa·sec; v = interstitial flow velocity, 1.881
916 × 10^{-4} m/sec; and σ = interfacial tension between methane and brine, ~70
917 mN/m) is calculated under the current experimental condition shown in
918 Tables 1 and 2. Such a low N_c (< 10^{-5}) suggests that capillary forces are
919 dominant for the fluid flow in the specimen as compared to viscous forces.
920 The low capillary number (N_c = ~3.316 × 10^{-8}) combined with the
921 unfavorable viscosity ratio (M = 8.452 × 10^{-3} < 1) reveal that capillary
922 fingering likely occurs during the relative permeability test (Lenormand,
923 1990; Lenormand et al., 1988; Sinha and Wang, 2007). Also note that the
924 unfavorable viscosity ratio may cause the relative permeability of displaced
925 fluid (brine) to be underestimated from its true value which is generally
926 considered to be obtained with the steady-state method (Maini et al., 1990).

927 In typical sandy HBS constituting high quality reservoirs, the
928 irreducible water saturations typically exist within a range of 0.05-0.30 based

on interpretations of NMR-log data (Myshakin et al., 2011). Those numbers represent capillary-bound, clay-bound, and structural water that is considered immobile over a time period of gas production from a hydrate reservoir. The high numbers of residual (or pseudo irreducible) brine saturation found in this pore-scale laboratory test preclude direct application of the deduced relative permeability data in reservoir simulations. Increasing the viscous force by applying a higher methane injection flow rate may reduce the high residual brine saturation values shown in Figure 8. The higher injection flow rate will increase the ΔP across the specimen and may also reduce the effect of capillary heterogeneity on the high residual brine saturation by allowing the injected methane to invade smaller pore spaces. However, the application of a higher injection flow rate should be carried out in consideration of higher potential of particle migration in the specimen, turbulent flow, and extra hydrate formation especially at the inlet face of the specimen, as well as the capacity of instruments for larger flow rate and volume.

8. Summary and Conclusion

This work is one of the first experimental studies of two-phase (methane-brine) flow in brine-saturated HBS samples prepared to mimic natural settings and proposes a novel experimental system and procedure to obtain relative permeability of gas (methane) and liquid (brine) in HBS. This study discusses **1)** technical challenges in conducting the gas-liquid relative

permeability test on HBS, **2)** experimental methodology and setup to overcome the technical challenges, **3)** preparation of a sandy HBS specimen with a natural-like pore habit and execution of single-phase (brine) permeability and gas-liquid (methane-brine) relative permeability tests, particularly the latter with the unsteady-state drainage displacement method, and **4)** estimation of the relative permeability curves and residual saturation calculated by Buckley-Leverett (B-L)-theory-based Toth's method (Toth et al., 1998; Toth et al., 2002).

The most difficult experimental challenge for a successful gas-liquid relative permeability test on HBS is to maintain the initial hydrate saturation and configuration under the dynamic flow condition. Key approaches used to maintain the hydrate saturation in this study include:

- Using brine (5 wt % $CaCl_2$) to saturate the specimen,
- Applying the test P-T condition (6.89-7.10 MPa and 7.8-8.4 °C) set slightly outside the hydrate stability boundary (6.89 MPa and 7.7 °C) at the salinity level used in brine,
- Pre-equilibrating methane and brine with each other under the test P-T condition before their injection into the specimen.

Other experimental solutions to conduct reliable gas-liquid relative permeability tests on HBS are also proposed in this study as follows:

Instrumental solutions for better maintenance of the applied P-T condition

are:

- A large liquid reservoir (1.5-liter) installed before the back pressure regulator to reduce the pore pressure fluctuations,
- A cold room to accommodate the entire test setup under the controlled temperature condition,
- Additional cooling jacket on the pressure chamber for temperature control of the specimen.

Approaches to avoid hydrate clogging in flow lines are:

- Covering tubing lines with insulation materials to avoid direct exposure to ambient cooling air of the environmental chamber,
- Using spot heating sources, such as heating tip, gun, or even warming by hand, to heat up the hydrate-clogging-prone sections, such as ΔP pressure line loop and downstream flow line,
- Using high salinity brine (8 wt % $CaCl_2$) to fill up the 1.5-liter reservoir to avoid hydrate clogging in the downstream line up to the back-pressure regulator.

Solutions for other challenges are:

- Using high-pressure sonic phase separator to measure the volume of displaced fluid under the test P-T condition for accuracy,
- Saturating the specimen with $CaCl_2$ brine to limit clay migration by forming larger clay flocs and using a paper filter (Grade P5; particle

retention = 5 to 10 μm) to prevent any particle loss from the specimen,

- Selecting a high gas injection flow rate from the near-wellbore area of a simulated producing reservoir to reduce the adverse capillary effects on the relative permeability test results.

While overcoming many technical difficulties associated with conducting the unsteady-state relative permeability test in HBS, this study reveals the low displacement efficiency in HBS resulting in high residual brine saturations. Besides the viscous instability which is inherent for any gas-liquid drainage displacement tests, one possible reason for the low displacement efficiency in HBS compared to HFS can be the shift of a pore size distribution toward a wide range due to the appearance of small pores in the presence of hydrate. Consequently, a strong capillary heterogeneity can develop in HBS likely contributing to the high residual saturation. The verification of this issue is outside the scope of this study, but it is worthy of investigation in future. The results obtained in this work and summarized above, nevertheless, pave a way to further improvements of experimental apparatus and test execution framework, and bring the understanding of the complex two-phase flow phenomenon in HBS.

Further improvements on the test setup and method in future may include **1)** improvement on controlling gas injection flow rate for the drainage displacement test: it is hard to smoothly increase the gas injection

flow rate to a targeted level without an overshoot with the current MFC, **2)** increase in size of brine reservoir that is used to reduce the fluctuation of back pressure: the total amount of gas injection can be limited within 1.5 liter with the current reservoir; and **3)** improvement on temperature control in the environmental chamber: a temperature fluctuation of the chamber causes the fluctuation of the specimen temperature and may lead to the unintended hydrate formation in flow lines.

Upon the experimental results observed in this study, the future investigation may involve **1)** inverse modeling simulations to calculate curve fitting parameters of conventional or newly developed relative permeability models using obtained test results, **2)** further relative permeability tests with higher flow rates of methane injection to mitigate the effect of capillary heterogeneity on the results, and **3)** experimental measurements of wettability of hydrates with respect to brine under equilibrium conditions of brine-hydrate-methane.

Credit Author Statement

Jeong-Hoon Choi, Conceptualization, Methodology, Formal analysis, Investigation, Writing - original draft, Writing - review & editing. Evgeniy M. Myshakin, Formal analysis, Writing - review & editing. Liang Lei, Validation, Writing - review & editing. Timothy J. Kneafsey, Validation, Writing - review & editing. Yongkoo Seol, Conceptualization, Resources, Writing - review & editing, Supervision, Funding acquisition.

Acknowledgements

This work was performed in support of the US Department of Energy's Fossil Energy Crosscutting Technology Research Program. The Research was executed through the NETL Research and Innovation Center's Hydrate Research Field Work Proposal. Research performed by Leidos Research Support Team (LRST) staff was conducted under the RSS contract 89243318CFE000003. We thank Karl Jarvis (LRST) for his technical support during the entire course of this experimental effort. We have no data sharing issues, and all the experimental/analytical data referenced in this article are accessible through the shown figures, tables, and references.

Disclaimer

This work was funded by the Department of Energy, National Energy Technology Laboratory, an agency of the United States Government, through a support contract with Leidos Research Support Team (LRST). Neither the United States Government nor any agency thereof, nor any of their employees, nor LRTS, nor any of their employees, makes any warranty, expressed or implied, or assumes any legal liability or responsibility for the accuracy, completeness, or usefulness of any information, apparatus, product, or process disclosed, or represents that its use would not infringe privately owned rights. Reference herein to any specific commercial product, process, or service by trade name, trademark, manufacturer, or

otherwise, does not necessarily constitute or imply its endorsement, recommendation, or favoring by the United States Government or any agency thereof. The views and opinions of authors expressed herein do not necessarily state or reflect those of the United States Government or any agency thereof.

References

Ahn, T., Lee, J., Huh, D.-G., Kang, J.M., 2005. Experimental study on two-phase flow in artificial hydrate-bearing sediments. Geosystem Engineering 8, 101-104.

Anderson, B.J., Kurihara, M., White, M.D., Moridis, G.J., Wilson, S.J., Pooladi-Darvish, M., Gaddipati, M., Masuda, Y., Collett, T.S., Hunter, R.B., Narita, H., Rose, K., Boswell, R., 2011. Regional long-term production modeling from a single well test, Mount Elbert gas hydrate stratigraphic test well, Alaska North slope. Marine and Petroleum Geology 28, 493-501.

Boswell, R., 2009. Engineering. Is gas hydrate energy within reach? Science 325, 957-958.

Boswell, R., Schoderbek, D., Collett, T.S., Ohtsuki, S., White, M., Anderson, B.J., 2017. The Igínik Sikumi field experiment, Alaska North Slope: Design, operations, and implications for CO_2-CH_4 exchange in gas hydrate reservoirs. Energy & Fuels 31, 140-153.

Boswell, R., Shelander, D., Lee, M., Latham, T., Collett, T., Guerin, G., Moridis, G., Reagan, M., Goldberg, D., 2009. Occurrence of gas hydrate in Oligocene Frio sand: Alaminos Canyon Block 818: Northern Gulf of Mexico. Marine and Petroleum Geology 26, 1499-1512.

Buckley, S.E., Leverett, M.C., 1942. Mechanism of fluid displacement in sands. Transactions of the AIME 146, 107-116.

Choi, J.-H., Dai, S., Cha, J.H., Seol, Y., 2014. Laboratory formation of noncementing hydrates in sandy sediments. Geochemistry, Geophysics, Geosystems 15, 1648-1656.

Collett, T.S., Johnson, A.H., Knapp, C.C., Boswell, R., 2009. Natural gas hydrates: A review, in: Collett, T., Johnson, A., Knapp, C., Boswell, R. (Eds.), Natural gas hydrates—Energy resource potential and associated geologic hazards: AAPG Memoir 89. The American Association of Petroleum Geologists (AAPG), pp. 146–219.

Dai, S., Santamarina, J.C., 2014. Sampling disturbance in hydrate-bearing sediment pressure cores: NGHP-01 expedition, Krishna–Godavari Basin example. Marine and Petroleum Geology 58, 178-186.

Dai, S., Seol, Y., 2014. Water permeability in hydrate-bearing sediments: A pore-scale study. Geophysical Research Letters 41, 4176–4184.

Dallimore, S.R., Collett, T.S., Taylor, A.E., Uchida, T., Weber, M., Chandra, A., Mroz, T.H., Caddel, E.M., Inoue, T., 2005. Scientific results from the Mallik 2002 gas hydrate production research well program, Mackenzie Delta, northwest territories, Canada: Preface. Bulletin of the Geological Survey of Canada 585.

Deaton, W.M., Frost, E.M., 1946. Gas hydrates and their relation to the operation of natural-gas pipelines. Bureau of Mines, U.S. Department of the Interior, Washington, D. C., p. 101.

Delli, M.L., Grozic, J.L.H., 2014. Experimental determination of permeability of porous media in the presence of gas hydrates. J Petrol Sci Eng 120, 1-9.

1114 Dow, 1966. Calcium Chloride Handbook. Dow Chemical Company.

1115 Han, G., Kwon, T.-H., Lee, J.Y., Jung, J., 2020. Fines migration and pore clogging
1116 induced by single- and two-phase fluid flows in porous media: From the
1117 perspectives of particle detachment and particle-level forces. Geomechanics for
1118 Energy and the Environment 23, 100131.

1119 Honarpour, M., Koederitz, L., Harvey, A.H., 1986. Relative permeability of petroleum
1120 reservoirs. CRC Press, Inc., Boca Raton, Florida.

1121 Hunt, J.R., Sitar, N., Udell, K.S., 1988. Nonaqueous phase liquid transport and
1122 cleanup: 1. Analysis of mechanisms. Water Resources Research 24, 1247-1258.

1123 Huppler, H.D., 1970. Numerical investigation of the effects of core heterogeneities
1124 on waterflood relative permeability. Society of Petroleum Engineers Journal 10,
1125 381-392.

1126 Ito, T., Komatsu, Y., Fujii, T., Suzuki, K., Egawa, K., Nakatsuka, Y., Konno, Y., Yoneda,
1127 J., Jin, Y., Kida, M., Nagao, J., Minagawa, H., 2015. Lithological features of
1128 hydrate-bearing sediments and their relationship with gas hydrate saturation in
1129 the eastern Nankai Trough, Japan. Marine and Petroleum Geology 66, 368-378.

1130 Jaiswal, N.J., 2004. Measurement of gas-water relative permeabilities in hydrate
1131 systems, Petroleum Engineering. University of Alaska, Fairbanks, Alaska, USA, p.
1132 100.

1133 Johnson, A., Patil, S., Dandekar, A., 2011. Experimental investigation of gas-water
1134 relative permeability for gas-hydrate-bearing sediments from the Mount Elbert
1135 Gas Hydrate Stratigraphic Test Well, Alaska North Slope. Marine and Petroleum
1136 Geology 28, 419-426.

1137 Johnson, E.F., Bossler, D.P., Naumann, V.O., 1959. Calculation of relative
1138 permeability from displacement experiments. Petroleum Transactions, AIME
1139 216, 370-372.

1140 Jones, S.C., Roszelle, W.O., 1978. Graphical techniques for determining relative
1141 permeability from displacement experiments. Journal of Petroleum Technology
1142 30, 807-817.

1143 Katsuki, D., Ohmura, R., Ebinuma, T., Narita, H., 2007. Methane hydrate crystal
1144 growth in a porous medium filled with methane-saturated liquid water.
1145 Philosophical Magazine 87, 1057-1069.

1146 Konno, Y., Jin, Y., Yoneda, J., Kida, M., Egawa, K., Ito, T., Suzuki, K., Nagao, J., 2015a.
1147 Effect of methane hydrate morphology on compressional wave velocity of sandy
1148 sediments: Analysis of pressure cores obtained in the Eastern Nankai Trough.
1149 Marine and Petroleum Geology 66, 425-433.

1150 Konno, Y., Yoneda, J., Egawa, K., Ito, T., Jin, Y., Kida, M., Suzuki, K., Fujii, T., Nagao,
1151 J., 2015b. Permeability of sediment cores from methane hydrate deposit in the
1152 Eastern Nankai Trough. Marine and Petroleum Geology 66, 487-495.

1153 Kumar, A., Maini, B., Bishnoi, P.R., Clarke, M., Zatsepina, O., Srinivasan, S., 2010.
1154 Experimental determination of permeability in the presence of hydrates and its
1155 effect on the dissociation characteristics of gas hydrates in porous media. J
1156 Petrol Sci Eng 70, 114-122.

1157 Lei, L., Seol, Y., Choi, J.-H., Kneafsey, T.J., 2019. Pore habit of methane hydrate and

its evolution in sediment matrix - Laboratory visualization with phase-contrast micro-CT. Marine and Petroleum Geology 104, 451-467.

Lei, L., Seol, Y., Jarvis, K., 2018. Pore-scale visualization of methane hydrate-bearing sediments with micro-CT. Geophysical Research Letters 45, 5417-5426.

Lenormand, R., 1990. Liquids in porous media. Journal of Physics: Condensed Matter 2, SA79–SA88.

Lenormand, R., Touboul, E., Zarcone, C., 1988. Numerical models and experiments on immiscible displacements in porous media. Journal of Fluid Mechanics 189, 165–187.

Li, J.-F., Ye, J.-L., Qin, X.-W., Qiu, H.-J., Wu, N.-Y., Lu, H.-L., Xie, W.-W., Lu, J.-A., Peng, F., Xu, Z.-Q., Lu, C., Kuang, Z.-G., Wei, J.-G., Liang, Q.-Y., Lu, H.-F., Kou, B.-B., 2018. The first offshore natural gas hydrate production test in South China Sea. China Geology 1, 5-16.

Liang, H., Song, Y., Chen, Y., Liu, Y., 2011. The measurement of permeability of porous media with methane hydrate. Petroleum Science and Technology 29, 79-87.

Mahabadi, N., Dai, S., Seol, Y., Yun, T.S., Jang, J., 2016. The water retention curve and relative permeability for gas production from hydrate-bearing sediments: pore-network model simulation. Geochemistry, Geophysics, Geosystems 17, 3099–3110.

Mahabadi, N., Jang, J., 2014. Relative water and gas permeability for gas production from hydrate-bearing sediments. Geochemistry, Geophysics, Geosystems 15, 2346-2353.

Maini, B., Coskuner, G., Jha, K., 1990. A comparison of steady-state and unsteady-state relative permeabilities of viscous oil and water in Ottawa sand. Journal of Canadian Petroleum Technology 29, 72-77.

Makogon, Y.F., Holditch, S.A., Makogon, T.Y., 2007. Natural gas hydrates — A potential energy source for the 21st Century. J Petrol Sci Eng 56, 14-31.

Moridis, G.J., Silpngarmlert, S., Reagan, M.T., Collett, T., Zhang, K., 2011. Gas production from a cold, stratigraphically-bounded gas hydrate deposit at the Mount Elbert Gas Hydrate Stratigraphic Test Well, Alaska North Slope: Implications of uncertainties. Marine and Petroleum Geology 28, 517-534.

Myshakin, E.M., Anderson, B.J., Rose, K., Boswell, R., 2011. Simulations of variable bottom hole pressure regimes to improve production from the double-unit Mount Elbert, Milne Point Unit, North Slope Alaska hydrate deposit. Energy & Fuels 25, 1077-1091.

Myshakin, E.M., Jiang, H., Warzinski, R.P., Jordan, K.D., 2009. Molecular dynamics simulations of methane hydrate decomposition. Journal of Physical Chemistry A 113, 1913-1921.

Myshakin, E.M., Seol, Y., Lin, J.-S., Uchida, S., Collett, T.S., Boswell, R., 2019. Numerical simulations of depressurization-induced gas production from an interbedded turbidite gas hydrate-bearing sedimentary section in the offshore India: Site NGHP-02-16 (Area-B). Marine and Petroleum Geology 108, 619-638.

NIST, 2018. Thermophysical Properties of Fluid Systems, NIST Chemistry WebBook,

SRD 69. National Institute of Standards and Technology, U.S. Department of Commerce.

Oyeneyin, M.B., Peden, J.M., Hosseini, A., Ren, G., 1995. Factors to consider in the effective management and control of fines migration in high permeability sands, SPE European Formation Damage Conference, The Hague, Netherlands.

Peters, E.J., 2012. Advanced petrophysics: Dispersion, interfacial phenomena/wettability, capillarity/capillary pressure, relative permeability. Live Oak Book Company, Austin, TX.

Peters, E.J., Khataniar, S., 1987. The effect of instability on relative permeability curves obtained by the dynamic-displacement method. SPE Formation Evaluation 2, 469-474.

Priest, J.A., Rees, E.V.L., Clayton, C.R.I., 2009. Influence of gas hydrate morphology on the seismic velocities of sands. Journal of Geophysical Research 114, B11205.

Rees, E.V.L., Kneafsey, T.J., Seol, Y., 2011. Methane hydrate distribution from prolonged and repeated formation in natural and compacted sand samples: X-ray CT observations. Journal of Geological Research 2011, 1-15.

Richardson, J.G., Kerver, J.K., Hafford, J.A., Osoba, J.S., 1952. Laboratory determination of relative permeability. Petroleum Transactions, AIME 195, 187-196.

Sakamoto, Y., Komai, T., Kawabe, Y., Tenma, N., Yamaguchi, T., 2004. Formation and dissociation behavior of methane hydrate in porous media — Estimation of permeability in methane hydrate reservoir, Part1. Shigen-to-Sozai 120, 85-90.

Santamarina, J.C., Dai, S., Terzariol, M., Jang, J., Waite, W.F., Winters, W.J., Nagao, J., Yoneda, J., Konno, Y., Fujii, T., Suzuki, K., 2015. Hydro-bio-geomechanical properties of hydrate-bearing sediments from Nankai Trough. Marine and Petroleum Geology 66, 434-450.

Schembre, J.M., Kovscek, A.R., 2003. A technique for measuring two-phase relative permeability in porous media via X-ray CT measurements. J Petrol Sci Eng 39, 159-174.

Schoderbek, D., Farrell, H., Hester, K., Howard, J., Raterman, K., Silpngarmlert, S., Martin, K.L., Smith, B., Klein, P., 2013. ConocoPhillips gas hydrate production test final technical report, Oil & Natural Gas Technology. National Energy Technology Laboratory, United States Department of Energy, p. 204.

Seol, Y., Choi, J.-H., Dai, S., 2014. Multi-property characterization chamber for geophysical-hydrological investigations of hydrate bearing sediments. Review of Scientific Instruments 85, 084501.

Seol, Y., Kneafsey, T.J., 2011. Methane hydrate induced permeability modification for multiphase flow in unsaturated porous media. Journal of Geophysical Research: Solid Earth 116, B08102.

Seol, Y., Kneafsey, T.J., Tomutsa, L., Moridis, G.J., 2006. Preliminary relative permeability estimates of methane hydrate-bearing sand, TOUGH Symposium 2006. Lawrence Berkeley National Laboratory, Berkeley, California, USA.

Sharma, M.M., Chamoun, H., Sarma, D.S.H.S.R., Schechter, R.S., 1992. Factors

controlling the hydrodynamic detachment of particles from surfaces. Journal of Colloid and Interface Science 149, 121–134.

Sigmund, P.M., McCaffery, F.G., 1979. An improved unsteady state of procedure for determining the relative permeability characteristics of heterogeneous porous media. Society of Petroleum Engineers Journal 19, 15-28.

Singh, H., Mahabadi, N., Myshakin, E.M., Seol, Y., 2019. A mechanistic model for relative permeability of gas and water flow in hydrate-bearing porous media with capillarity. Water Resources Research.

Singh, H., Myshakin, E.M., Seol, Y., 2018. A nonempirical relative permeability model for hydrate-bearing sediments. Society of Petroleum Engineers Journal, SPE-193996-PA.

Sinha, P.K., Wang, C., 2007. Pore-network modeling of liquid water transport in gas diffusion layer of a polymer electrolyte fuel cell. Electrochimica Acta 52, 7936-7945.

Spangenberg, E., Kulenkampff, J., Naumann, R., Erzinger, J., 2005. Pore space hydrate formation in a glass bead sample from methane dissolved in water. Geophysical Research Letters 32, L24301.

Toth, J., Bodi, T., Szucs, P., Civan, F., 1998. Practical method for analysis of immiscible displacement in laboratory core tests. Transport in Porous Media 31, 347-363.

Toth, J., Bodi, T., Szucs, P., Civan, F., 2002. Convenient formulae for determination of relative permeability from unsteady-state fluid displacements in core plugs. J Petrol Sci Eng 36, 33-44.

Vega, B., Kovscek, A.R., 2014. Steady-state relative permeability measurements, temperature dependency and a reservoir diatomite core sample evolution, SPE Annual Technical Conference and Exhibition, Amsterdam, The Netherlands.

Wan, J., Tokunaga, T.K., 2002. Partitioning of clay colloids at air-water interfaces. Journal of Colloid and Interface Science 247, 54–61.

Welge, H.J., 1952. A simplified method for computing recovery by gas or water drive. Petroleum Transactions, AIME 195, 91-98.

White, M.D., Wurstner, S.K., McGrail, B.P., 2011. Numerical studies of methane production from Class 1 gas hydrate accumulations enhanced with carbon dioxide injection. Marine and Petroleum Geology 28, 546-560.

Yamamoto, K., 2013. Japan completes first offshore methane hydrate production test-Methane successfully produced from deepwater hydrate layers. Fire in the Ice 13, 1-2.

Yang, J., Tohidi, B., Chapoy, A., 2008. Impact of sedimentary mineralogy on the geophysical and geomechanical properties of hydrate-bearing sediments, 6th International Conference on Gas Hydrates, Vancouver, British Columbia, Canada.

Yoneda, J., Oshima, M., Kida, M., Kato, A., Konno, Y., Jin, Y., Jang, J., Waite, W.F., Kumar, P., Tenma, N., 2019. Permeability variation and anisotropy of gas hydrate-bearing pressure-core sediments recovered from the Krishna–Godavari Basin, offshore India. Marine and Petroleum Geology 108, 524-536.

Table 1. Core physical properties and experimental conditions.

Host sediment	silica sands (F110, mean particle size = 120μm) + 5 wt % kaolinite clays (mean particle size = 1μm)
Initial gravimetric water content, W (%)	9.3
Diameter × Length, $D \times L$ (mm)	50.8 × 153.7
Initial nominal pore volume, $V_{p,0}$ (ml)	109.6
Initial porosity, n_0	0.35
Hydrate saturation, S_h (%)	42.0
Pore pressure, u (MPa)	6.89
Temperature, T (°C)	~8
Effective confining stress, $\acute{\sigma}_o$ (MPa)	0.69

Table 2. Experimental parameters for permeability calculations.

Specimen		Hydrate-bearing (S_h = 42.0%)	Hydrate-free
Dynamic viscosity of brine, μ_{brine} (Pa·sec)		1.460E-03[a]	
Dynamic viscosity of methane, $\mu_{methane}$ (Pa·sec)		1.234E-05[b]	
Injection flow rates for single-phase perm. test, q_{brine} (ml/min)		0.5→1→0.5→2→1→4 →2→8→4→2→1→0.5	2→4→2→8→4→2
Effective permeability, k_e (mD)		148 (STDEV[c] = 7)	~
Intrinsic permeability, k_0 (mD)		~	795 (STDEV[c] = 71)
Injection flow rate for rel. perm. test, $q_{methane}$ (ml/min)		8	8
Effective pore volume[d], V_p (ml)		63.3	108.4
Statistical parameters	a (-)	0.816	0.801
	b (-)	14.714	2.895
	a_1 (Pa)	14095	16363
	b_1 (-)	-0.242	-0.209
Initial saturation of displacing fluid (methane), $S_{d,i}$ (-)		0	0

Note: [a] (Dow, 1966); [b] (NIST, 2018); [c] standard deviation; [d] effective pore volume = nominal pore volume – hydrate volume.

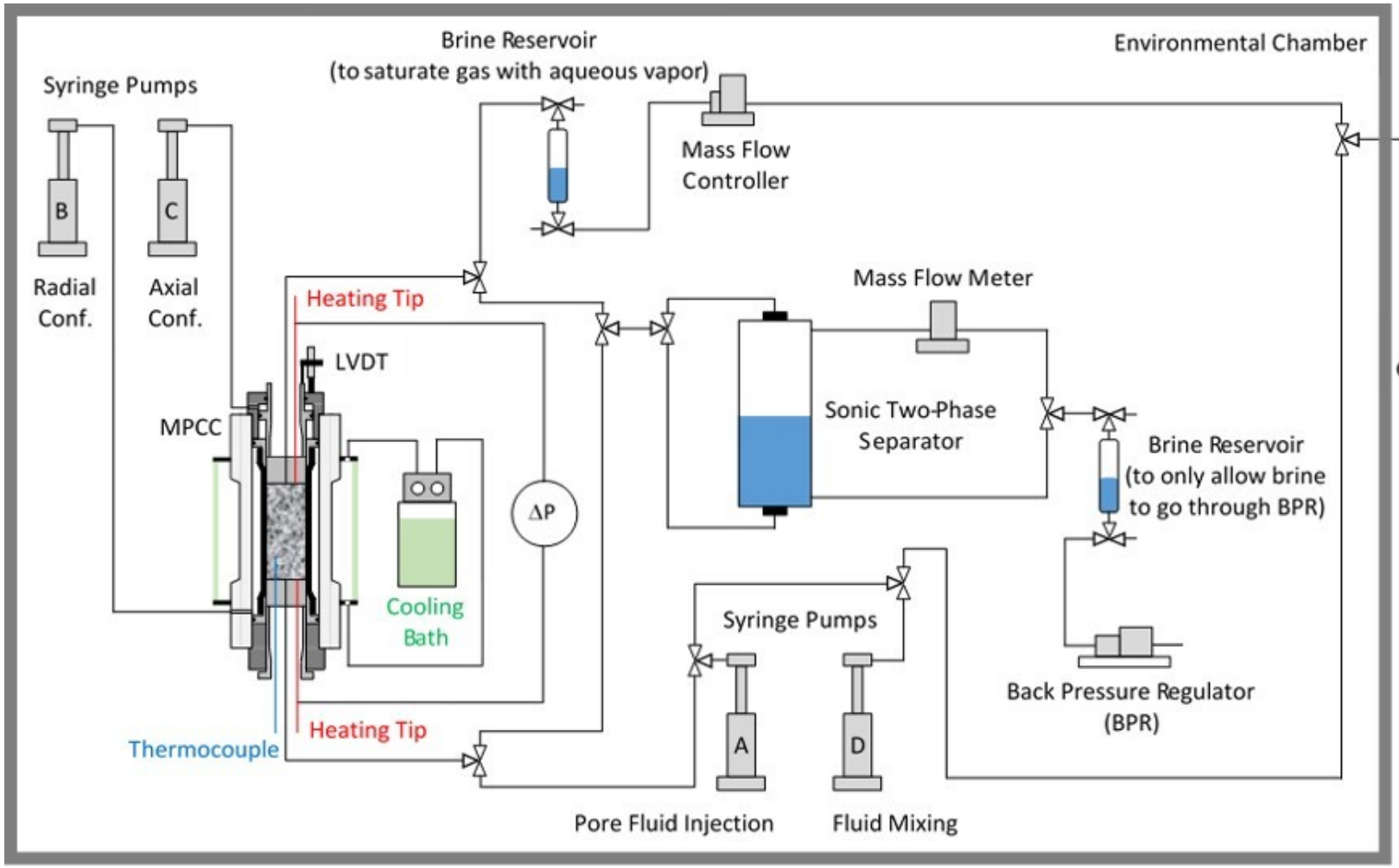

Figure 1. Schematic of experimental setup (MPCC: multi-property characterization chamber, and LVDT: linear variable differential transformer).

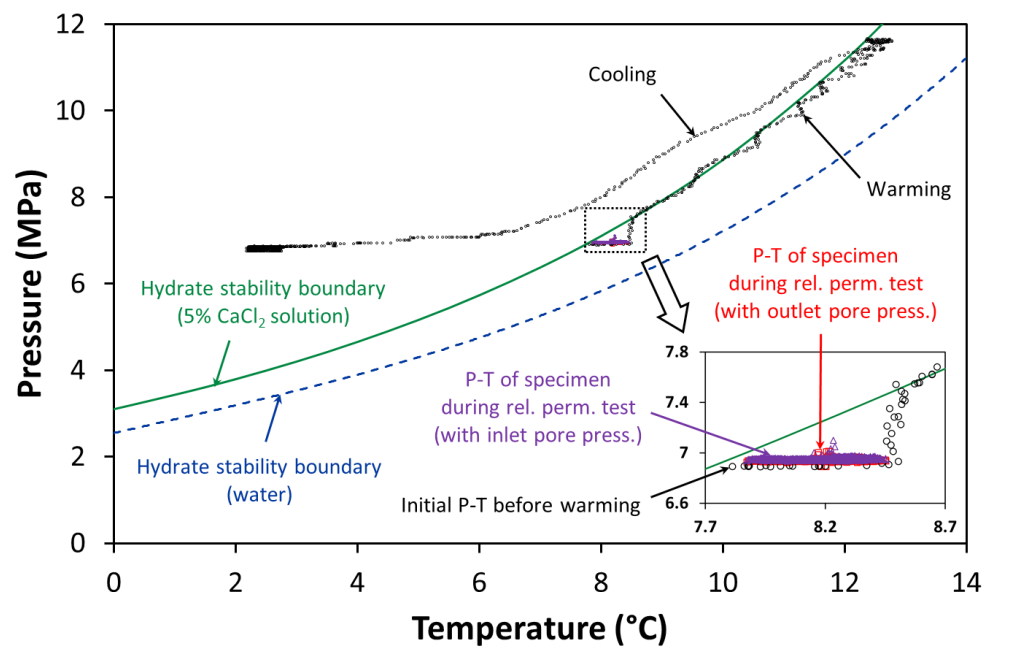

Figure 2. Pressure-temperature (P-T) of HBS specimen (S_h = 42.0%) during early warming-cooling process for specimen preparation and during relative permeability test. In the inset figure, black empty circles represent the P-T of specimen during early warming-cooling process, while the data in purple and red represent the P-T at inlet and outlet sides of specimen during relative permeability test, respectively.

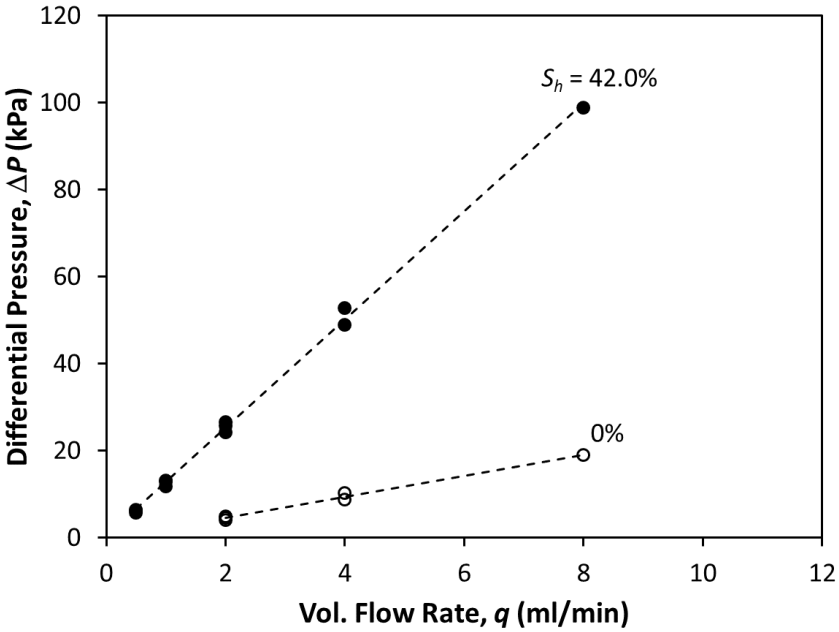

Figure 3. Variation of differential pressure (ΔP) across specimen at different volumetric injection flow rates (q) during single-phase (brine) permeability measurements: R^2-values of linear fittings (dashed lines) are > 0.990.

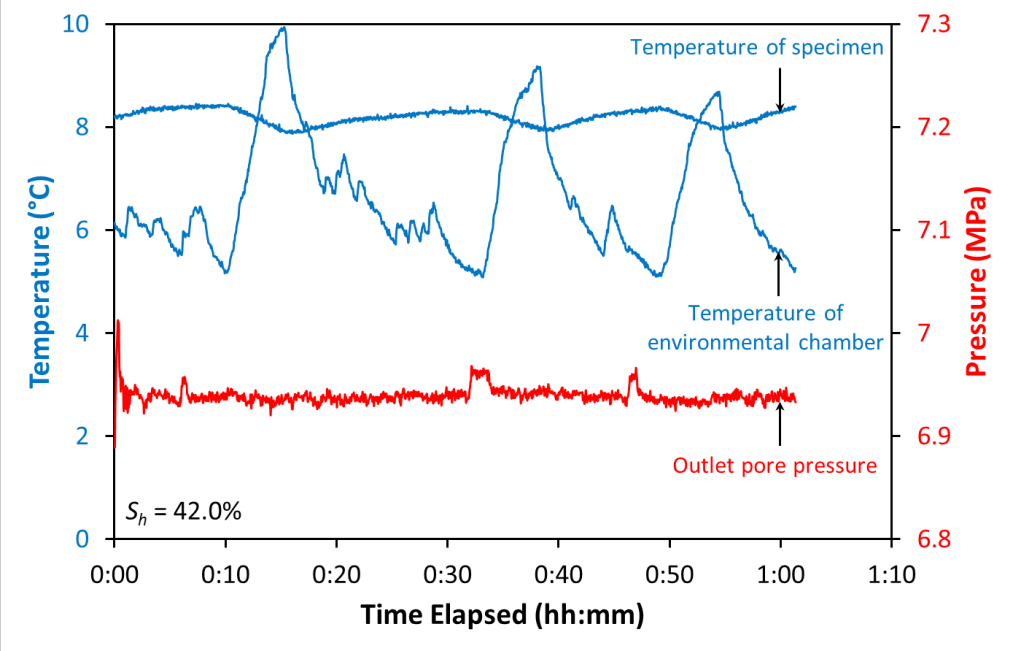

Figure 4. Pressure-temperature (P-T) of HBS specimen (S_h = 42.0%) and temperature of environmental chamber during relative permeability test.

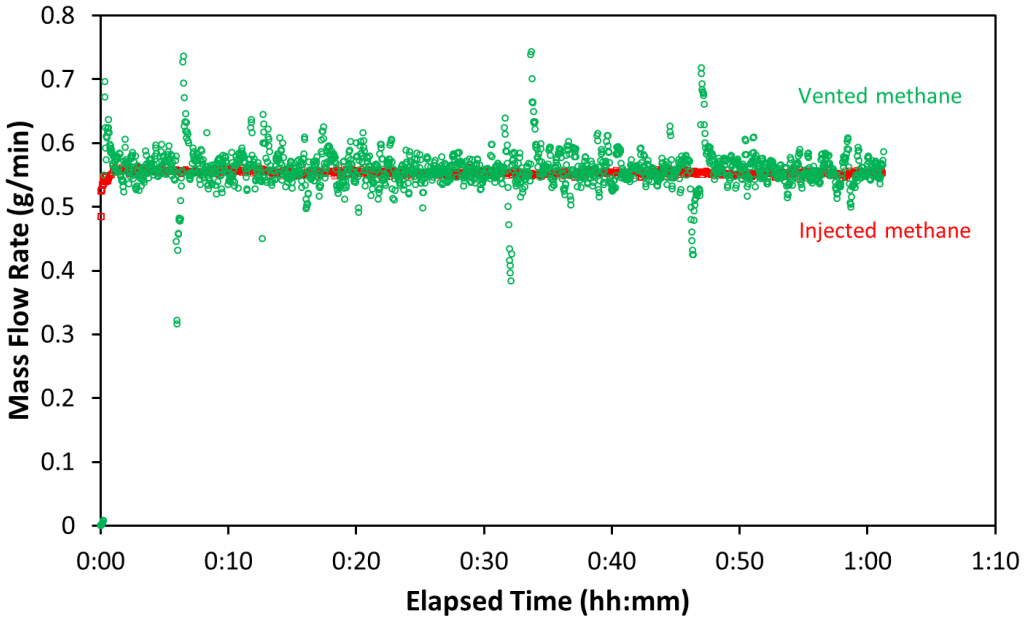

Figure 5. Mass balance between methane injected into the specimen and methane vented from upper outlet port of sonic fluid separator during relative permeability test on HBS specimen (S_h = 42.0%): The mass flow rate of vented methane is measured by the mass flow meter attached to the upper outlet port of sonic fluid separator (see Figure 1).

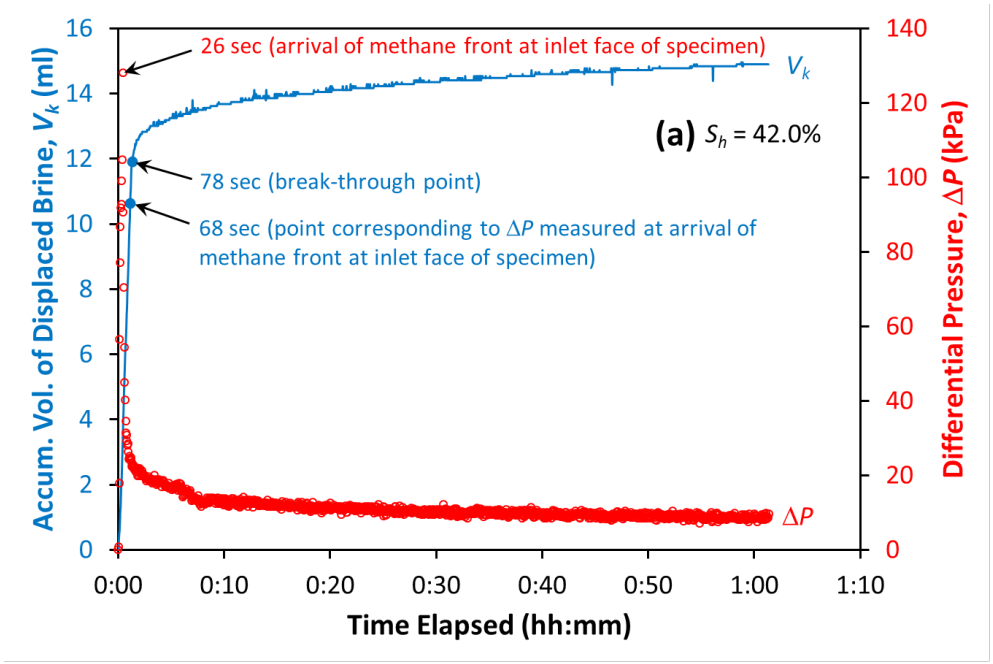

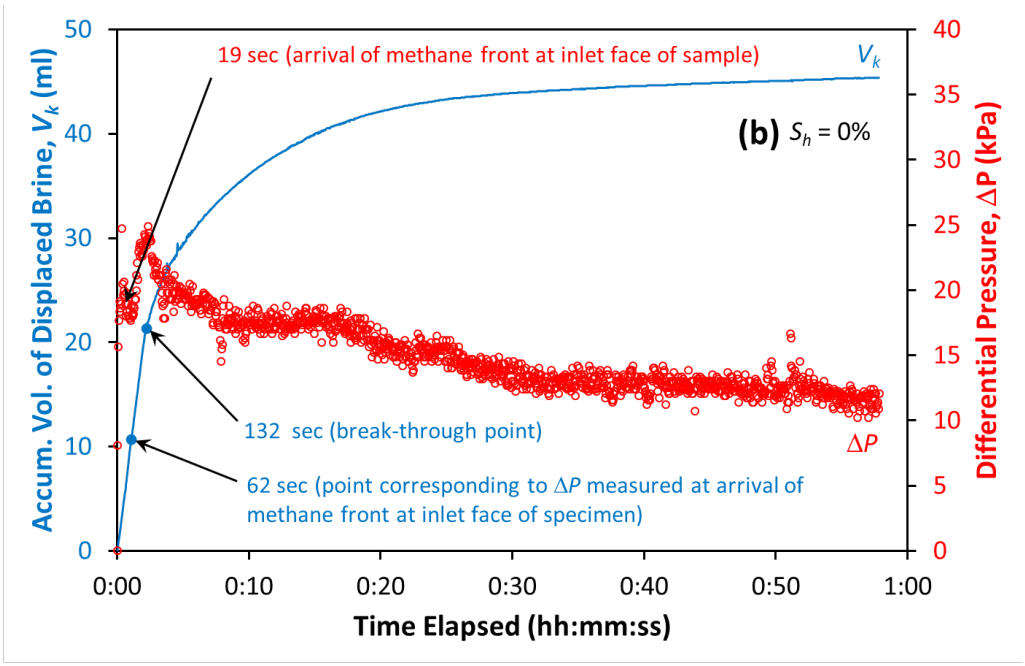

Figure 6. Differential pressure (ΔP) and accumulative volume of displaced brine (V_k) obtained during methane injection (at 8 ml/min) into **(a)** HBS specimen and **(b)** HFS specimen: The time is recorded from the onset of methane injection at the mass flow controller (MFC).

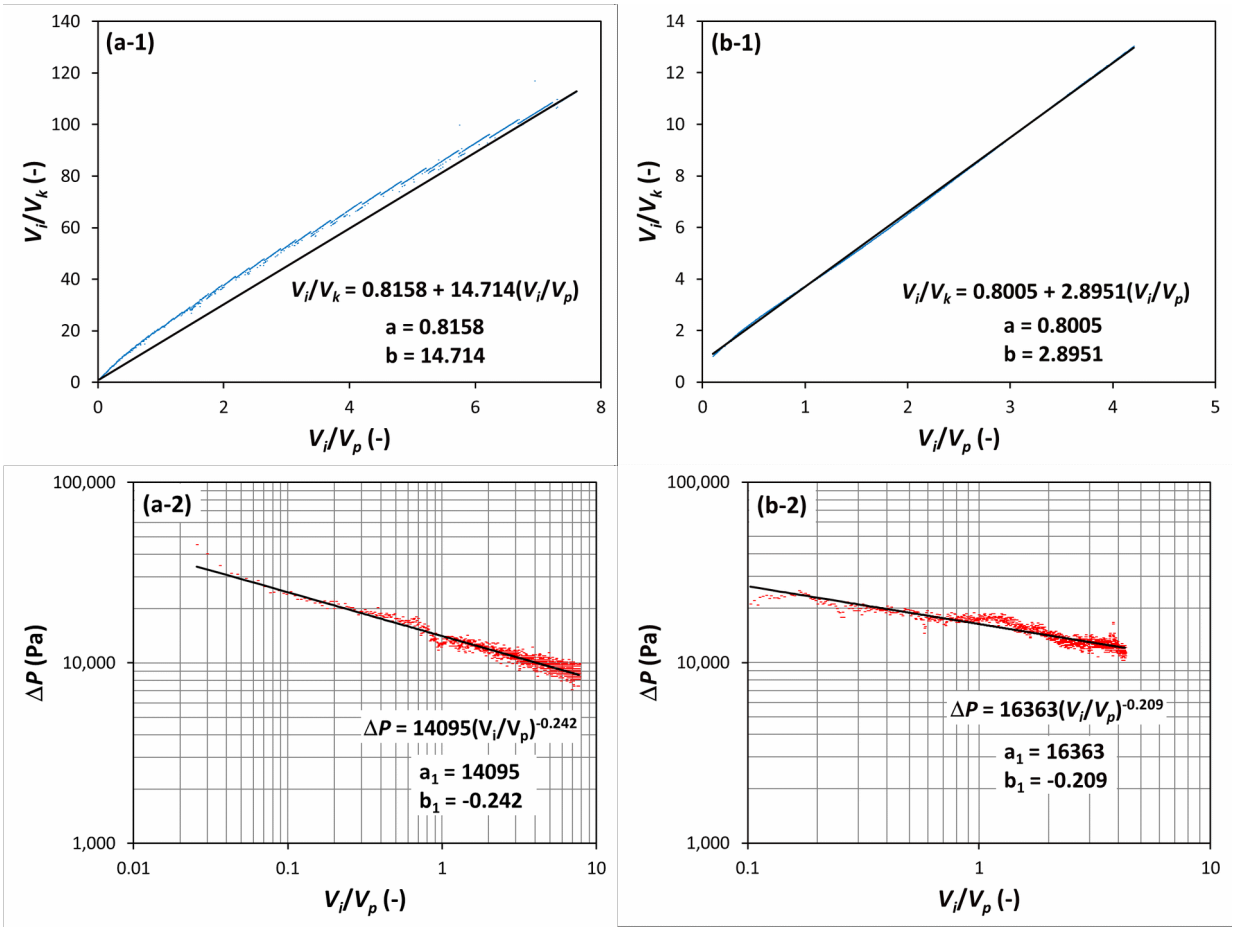

Figure 7. Trends of injected-to-displaced fluid volume ratio (V_i/V_k) and differential pressure across specimen (ΔP) vs. injected fluid-to-pore volume ratio (V_i/V_p) after break-through: **(a)** HBS specimen (S_h = 42.0%) and **(b)** HFS specimen. Note that ΔP vs. V_i/V_p trend is plotted in log-log scale. The empirical constants of a, b, a_1, and b_1 are to be utilized in the relative permeability calculation based on (Toth et al., 2002).

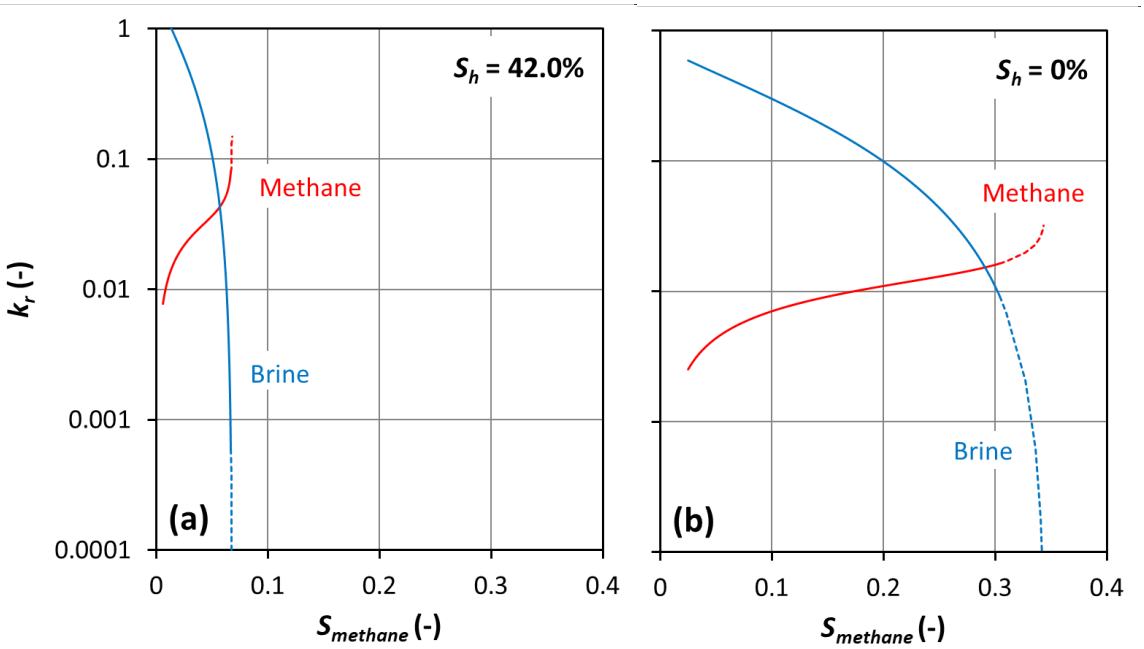

Figure 8. Relative permeability curves of **(a)** HBS specimen and **(b)** HFS specimen. Dotted lines represent the relative permeabilities extrapolated for 100 pore volumes (V_i/V_p) of methane injection.